Fingerprint-free Tracking with Dynamic Enhanced Field Division

Qingquan Zhang†, Ziqiao Zhou*, Wei Xu*, Jing Qi*, Chenxi Guo*, Ping Yi*, Ting Zhu†, Sheng Xiao‡
* Shanghai Jiao Tong University, Shanghai, China
† University of Maryland, Baltimore County, USA
‡ Hunan University, Hunan, China

***Abstract*—Wireless sensor networks are often deployed for tracking moving objects. Many tracking algorithms have been proposed with two general assumptions: the pre-set fingerprints(prior landmark or context information) and an interference-free environment. These algorithms, however, cannot be used for on-demand deployment where finger-prints are unavailable and would perform poorly in interference-rich environments. In this paper, we present a fingerprint-free localizing and tracking algorithm, called Enhanced Field Division (EFD). The EFD algorithm is used to dynamically divide the field into areas with unique signatures and tracks the target, without any finger-prints. We also implemented a proof-of-concept localization platform to demonstrate the tracking accuracy and the algorithm performance in practical, interference rich environment.**

I. Introduction

Wireless Sensor Networks (WSNs) have been widely used in military and civilian application for object tracking. [1] However, because of their cost and accuracy limitations, existing localization and tracking methods can hardly meet the performance requirements in large scale deployment [2].

In general, WSN-based localization mechanisms fall into two categories: range-free [3], [4] and range-based [5]. While the range-based methods require expensive hardware, precise model for Received Signal Strength (RSS) and dedicated analysis for noise [6], the range-free methods, demand for less range information, are more suitable for large-scale sensor network systems. The range-free strategy has been studied in many algorithms, such as Regulated Signature Distance(RSD) [7], Bubble Trace [8], EZ [9] and Unsupervised Indoor Localization(UnLoc) [10]. To skip the prerequisite of intensive prior study of the field by creating landmarks or fingerprints [10] for localization, we start our design by optimizing an influential factor – the deployment of the anchors.

In this paper, we first study the optimal deployment of the anchors and provide a new strategy for tracking, namely Enhanced Field Division (EFD), based on field signatures and dynamic divisions. Firstly, EFD ignores the actual value of the RSS and focuses on the high-low relationship between RSSs from each anchor, which is less affected by the RF fading than that with definite RSS value. Secondly, taking advantage of field division with optimal anchor placements, we avoid the issues of intensive fingerprint sampling. Thirdly, we present a novel tracking strategy, grid tracking, to further reduce tracking errors. With our aggressive dynamic localization strategy (defined and discussed in Section V-D) after matching the signature, the accuracy of localization can be enhanced efficiently. Finally, we build a localization system platform using off-the-shelf commercialized products.

The rest of the paper is organized as follows: Section II briefly describes the related works, and Section X concludes the paper; section III briefly describes the theoretic basis of the EFD; section IV lists the main challenges in existing location tracking methods; section V details the solutions and the system design; section VI analyzes the lesson learned; section VII evaluates the design with extensive simulations and make several comparisons with typical location tracking algorithm; section VIII introduces our test-bed system; section IX presents the experiments to demonstrate the effectiveness of the EFD.

II. Related Work

Localization in sensor networks has been a heating research topic recently [4], [5], [11]. Admittedly, this is not the first paper to use relative sequence instead of absolute values as an indication for localization. Sequence-based localization technique has been mathematically analyzed in [12]. Even in the ideal situation where anchors own the same peak RSS, the practical scenario will never reach the maximum number of subareas as their equations demonstrated, for they ignore the limitation between the boundaries and anchors, which is revealed by our work. Furthermore, the asymmetry of the RSS from different anchors caused the test-bed situation to be more complicated; our work deal with this problem effectively by using weighted sequence.

As for the measurement method, a continuum of algorithms exist across a variety of range-based and range-free configurations. Range-based algorithms use physical sensors or signal-strength mechanisms to detect motions. Most works [5], [11] use sensors and beacons to detect the movements for localization. Localization with signal-strength mechanisms such as Wi-Fi and GSM have been studied in the literature as well [13]. Later, grid-based methods were developed successfully and most of them rely on landmarks in school and office environments [10]. These methods determine the best landmarks for reliable localization. Recently, range-free localization [3], [4] were

developed, replacing landmarks with raw measurements and the histogram posterior with particles. In a hybrid of ideas between signal-strength mechanisms and grid-based methods, RSD [7] and RND [14] introduce novel range-free algorithms based on a relative distance using trilateration. Although the trilateration is indeed a remarkable universal method in tracking, the different models based on the trilateration result in different modifying factors.

This paper, thus, focuses on addressing the interference in common environments by replacing the trilateration with a map division and employing a close tracking technique for getting higher accuracy of localization, mainly making those contributions:

1) It is the first work trying to both optimize the anchor deployment for localization and consider the different peak signal value of anchors.
2) It breaks the traditional thinking of subareas in map segmentation by indicating the difference between subarea and sub-region.
3) It designs a C/S system to verify the algorithm in both friendly and unfriendly environments.
4) It proposes a dynamic dividing method to reduce estimated position bias in a static map.

III. Theoretic Basis of EFD

This section briefly describes two basic ideas, field signatures and division, in the EFD. Similar to the research in [7], we find that the relative RSS rather than the absolute one can be employed to mark different unique regions. We then introduce the concept of field division with which divided subarea owning a unique signature. Our discussion starts within a two-dimensional paradigm although the algorithm applies to a three-dimensional paradigm as well. [15] In this region, three heterogeneous wireless base stations (anchors), A, B and C are set in Fig. 1. Ignoring the environmental noise, RSS demonstrates a monotonic effect on the geographic distance [16]. Though using the relative value, we can support and improve with a well studied RSS distribution models in dbm (decibels above one milliwatt) as in Equation 1 [17] meets the purpose.

$$RSS = p_0 + 10n\log(\frac{r_0}{r}) \tag{1}$$

in which, n, r_0 and p_0 are the constants parameters, and r is the distance between the target and anchor. If r=r_0, RSS=p_0, letting k be the number of anchor nodes in a

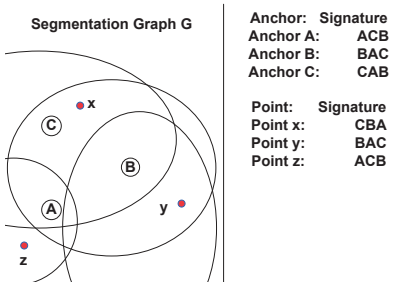

Fig. 1. An Example With Three Anchors

map, we define a high-dimensional location signature function $\mathcal{F}$ as follows:

$$s = \mathcal{F}(rss_1, rss_2), ..., rss_N)) \tag{2}$$

where s is signature of the target location, and rss_i, $1 \le i \le N$, is the target's RSS from the anchor node i. The function $\mathcal{F}$ is modeled by a descending sorting function. Therefore, we have $rss_i > rss_j$ for all $i < j$ for every signature s. Given the RSS transmission model, we denote the subarea in Definition 1 for field division and define the boundary as a curve that separating two adjacent subare as.

Definition 1 (Subarea)**.** *A subarea is the point set whose members own the same signature in the field segmentation.*

Taking a region with two anchors, A and B, as an example, point set belonging to the boundary (RSS_A=RSS_B) is derived as

$$p_{A0} + 10n\log\frac{r_{A0}}{r_A} = p_{B0} + 10n\log\frac{r_{B0}}{r_B} \tag{3}$$

where r_A and r_B represent the relative distance to anchor A and B. p_{A0}, p_{B0} is the reference RSS value at the distance of r_{A0}, r_{B0}. Solving this equation, we can get a relationship of r_A and r_B as

$$\frac{r_B}{r_A} = k, \text{where } k = 2^{\frac{p_{B0}-p_{A0}}{10n}}; \tag{4}$$

The point set, defined in Equation 4 (equal RSS from A and B), defines the Apollonius circle [18]. The circular arc (boundary) divides the area into two sub-regions so that every point on one side of the arc will see its RSS from anchor A to be stronger than that from B, and vice versa. Then a signature, s, for any given point can be decided immediately by its relative location toward the arc. For example, as shown in Fig. 1, the signature at position x, y and z will be $s_x = (C, B, A)$, $s_y = (B, A, C)$ and $s_z = (A, C, B)$ respectively. The signatures at anchors can be decided for consistency. At anchor point A, $s_A = (A, C, B)$. At anchor B, the $s_B = (B, A, C)$. Then the region is segmented into many subareas by signatures in Fig. 1.

Theorem 1. *In general, once the subareas are set, the signatures will be set and unique in each subarea.*

Proof of Theorem 1: If the signature of one subarea is not unique, there are two possible situations: Ether this signature will be found in at least one another subarea, or this subarea will own at least one other different signature. Then an apagogical method – we assume at least one possible situation will occur – can be used to illustrate our theorem. [7] ■

EFD wants to choose the placement of anchors to optimize the subarea generation. With this, we can estimate a target's location by judging the subarea in which the target lies by matching the signature created by the target to a pre-generated signature set S. As such, a new form of localization via subarea signature through optimal anchor deployment is created.

Then, the localization accuracy depends on the number of anchors N, the total number of signature subareas

and the anchor deployment. By using relative signal strength and thus unique signatures, we can alleviate the environmental interference suffered by traditional range-based techniques. Compared to a fingerprinting-based approach, which is time-consuming and vulnerable to infrastructure change, the EFD is cost-efficient and highly effective.

IV. Design Challenges

Though avoiding most of the intrinsic heavy burden or high infrastructure cost problems that happens in range-free methods, most range-based designs are faced with some challenges which will be solved in the EFD, such as calibrating the location system for different indoor surroundings or for real-time tracking, and positioning the wireless anchors to efficiently use signatures. Three main challenges for the proposed scheme are 1) vicious field divisions, 2) illegal signatures, and 3) status quo in tracking.

A. A Vicious Field Division

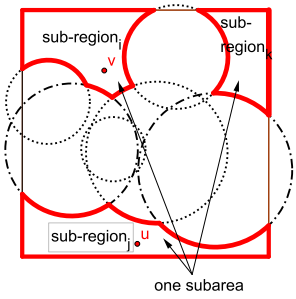

Fig. 2. Relationship between Sub-regions and Signatures

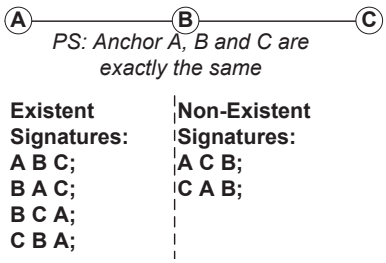

Fig. 3. The Example of Illegal Signatures in Linear Topology

Although the field division is lower-overhead and relatively accurate, some unexpected and vicious scenarios, which break the independence of the sub-regions, still remain. In practice, subarea and sub-region (defined in Definition 2) are similiar but not the same concepts in some scenarios that we will discuss in the following section.

Definition 2 (Sub-region)**.** *A sub-region is an area which is segmented by boundaries.*

As demonstrated previously, the ideal boundaries are arcs that define a continuous sub-region. However, a distracting scenario in which isolated sub-areas as one subarea (shown in Fig. 2) can be created due to unplanned anchor deployment. This issue forms our motivation to search for the optimal anchor deployments.

B. Illegal Signature

In order to intuitively understand the impact from RF fading and interference, we conducted a number of real-environmental measurements. What disturbed us most was that **illegal signatures** are derived from our signature function $\mathcal{F}$ based on the real-time sensing $\{rss(n_i)|i = 1, 2, ..., N\}$.

Definition 3 (Illegal Signature)**.** *An illegal signature is a signature that can not be mapped to any legitimate subarea based on the EFD's field division algorithm as we discussed previously.*

For example, as shown in Fig. 3, anchors A, B and C, the same in specification, are deployed in a linear topology; its legitimate signature set S includes only four signatures, $S = \{(A, B, C), (B, A, C), (B, C, A), (C, B, A)\}$. However, during real-environmental experiments, the signature function $\mathcal{F}$ reports $s = (A, C, B)$ or $s = (C, A, B)$. This happens when the RF fading and other environmental interference invalidate some segmentation based upon an ideal model defined in Equation 1. Hence, a need for a calibration design of the ideal RSS model for environment interference arises. We solve this challenge by combining the limited prior information and current sensing data to provide balanced field segmentation.

C. Status Quo Effects

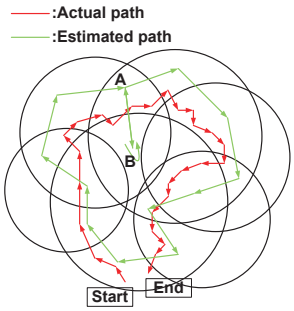

Fig. 4. Tracing without anchor deployment optimization

To increase the tracking accuracy, a certain amount of anchor coverage is preferred to provide larger field division. The effects of field heterogeneity resulting from random anchor deployment and insufficient anchor coverage can lead to the status quo problem, in which the system fails to track ground truth motions of the target, severely degrading measurement accuracy. As shown in Fig. 4, the target actually moves 26 steps, but basic signature presents only 14 positions. What's worse, when the target is leaping off the boundary–for example, the trail from point A to point B–the status quo situation will render a discontinuous tracking estimation. Obviously, the status quo problem embedded in a range-free based approach requires the tracking system to explore the motion information for improving tracking accuracy.

V. Basic System Design

In this section, specific solutions for the tasks mentioned in Section IV will be discussed, divided in five parts: field division, model adjustment, optimal anchor deployment, grid tracking strategy and correction when crossing the boundary.

A. Field Division

With the fundamental theory of the EFD, the physical information can be abstracted to the RSS signature for a region of interest once the anchors have been deployed. It should be emphasized that our design by nature does not rely on the accuracy of RSSs. The well-defined model presented as Equation 1 will suffice in our discussion.

More important to the EFD system is the accuracy and efficiency of signatures.

In a scenario with n anchors, the maximum number of signatures $M(n)$ could be calculated by Equation5 [7], where $\binom{n}{2}$ represents the number of circles

$$M(n) = \binom{n}{2}^2 - \binom{n}{2} + 2 \tag{5}$$

However, this equation still outnumbers the practical boundaries. Taking a group of three anchors α, β, γ as an example, B_1 is the boundary of α and β, B_2 is the boundary of α and γ, B_3 is the boundary of β and γ. $\bar{v\alpha}$ represent the distance of point v to point α, so are $\bar{v\beta}$, $\bar{v\gamma}$.

$$v \in B_1 \bigcap B_2 \Rightarrow \{ \begin{array}{l} \frac{\bar{v\alpha}}{\bar{v\beta}} = \frac{p_{v\alpha}}{p_\beta} \\ \frac{\bar{v\alpha}}{\bar{v\gamma}} = \frac{p_\alpha}{p_\gamma} \end{array} \tag{6}$$

$$\frac{\bar{v\beta}}{\bar{v\gamma}} = \frac{p_\beta}{p_\gamma} \Rightarrow v \in B_1 \bigcap B_2 \bigcap B_3 \tag{7}$$

In this way, B_1, B_2, B_3 owns only two points of intersection which is 4 less than that of three unlimited circles. So, the possible maximum partition is

$$\binom{n}{2}^2 - \binom{n}{2} + 2 - \frac{\binom{n}{3} * 4}{2} = \binom{n}{2}^2 - \binom{n}{2} - \binom{n}{3} * 2 + 2 \tag{8}$$

Increased number of anchors n leads to the growth of legitimate signatures or divisions, thus rendering higher localization resolutions. However, the challenge that the EFD addresses is to enhance localization accuracy under poor anchor coverage. Through the analysis above, the maximum number of legitimate signatures in a n-anchor map is less than $n!$, the total number of possible signature permutation.

Lemma 1. *$n! > M(n)$, when $n >= 5$;*

Given Lemma 1, we will encounter the illegal signature issue which will be addressed in Section IV-B.

B. Model Adjustment

Note that not the absolute value but rather the relative strength of RSS is relied in the EFD algorithm. Based on our measurements, we discovered the RSS degradation due to the impact of interference toward different anchors to be highly correlated. To accommodate RF fading and the multipath effects in environments, we can make an adjustment to the RSS model in Equation 1 for the sake of convenience. Therefore, we model the effects by a factor λ to p_0 so that $\lambda_i p_0$ absorbs the environmental interference pattern. The ideal RSS model shall be adjusted as:

$$RSS(i) = \lambda_i p_0 + 10nlog(\frac{r_0}{r_i}) + \epsilon \tag{9}$$

, where λ_i is the interference factor of anchors and ϵ is the adjustment error. Because factors $\lambda_i, i = 1, 2, ...N$, are highly correlated, the huge interference doesn't make much difference in the division signatures after adjusting the model. As a result, the problem turns into estimating λ_i to minimize the estimation $\sigma(\epsilon)$. If we denote $p^{'} = \lambda_i p_0$, and assume the $p^{'}$ follows a normal distribution, $p^{'} \sim N(\mu_0, \sigma_0^2)$, and there are prior beliefs about the $E(p^{'}) = \mu_0$, and $\sigma(p^{'}) = \sigma_0$, μ_0 and σ_0 represent the best guess for $p^{'}$, and the uncertainty of the guess, which comes from prior experiments or specification from service providers, we can modify the inputs to Equation 9 based on the in-situ estimation of $\hat{p^{'}}$ and $\hat{\sigma}(p^{'})$. [19] A standard estimator of expectations is the sample mean $\sigma(\epsilon)$

$$\hat{\mu} = \frac{1}{l} \sum_{t=1}^{l} X_T \sim N(\mu_1, \frac{\sigma_1^2}{l}) \tag{10}$$

, where l is the number of available sampling series. However, the sample mean is an inefficient estimator as the sampling estimation varies widely for different sampling series [19]. One way to cope with this issue is to use a more efficient *balance* estimator:

$$\mu^{(b)} \equiv (1 - b)\hat{\mu} + b\pi^0 \tag{11}$$

, where π^0 is our best guess, $\pi^0 \sim N(\mu_0, \sigma_0^2)$, and $0 \leq b \leq 1$ is the balance factor. The purpose is then to minimize balance σ_b under any given $\mu^{(b)}$. Thus,

$$\begin{array}{c} \text{Minimize } \sigma_b^2 = b'Vb \\ \text{Subject to } E(\mu_0) = b'U = \bar{\mu} \\ \sum_{i=1}^{n} b_i = 1 \end{array} \tag{12}$$

, where V is the covariance matrix between $\hat{\mu}$ and π^0, and U is the vector $[\mu_0, \mu_1]$.

The first solution to that formalization is

$$Vb = \lambda U, \rightarrow b = \lambda V^{-1} U$$

Thus, the optimal balance factors given by the answer are used to derive the $u^{(b)}$, as the optimal representation of $\lambda_i p_0$ in Equation 9.

C. Anchor Deployment

Signatures provide useful location information for practical tracking. The EFD algorithm also seeks to optimize its usage by avoiding the vicious division resulting from the complexity in signature mapping.

Theorem 2. *One subarea always owns only one signature, but one signature may owns more than one sub-region.*

Proof for Theorem 2:

(1) A target crosses one circle boundary for t times. If t is an odd, which means that two movements–leaving and entering that circle boundary–are paired, the sequence will not change;

(2) If v_j, v_k belong to the same subarea, v_j must cross each boundary t times (t=0, 2, 4, ...) to reach v_k.

Thus, one subarea owns only one signature.

(3) With asymmetrical p_0 and equal r_0 in Equation 9, boundaries are circles. It is possible that sub-region SR_i

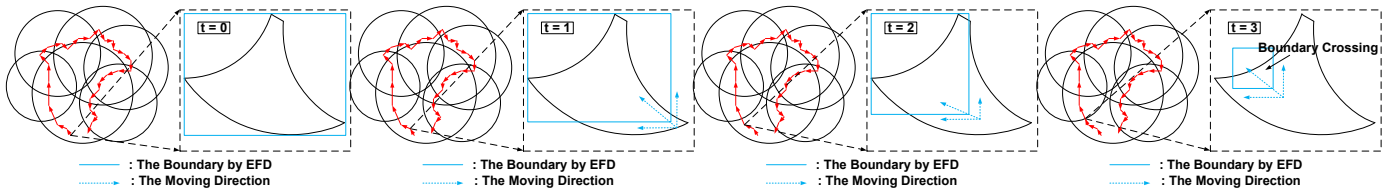

(a) t = 0, moving in subarea (b) t = 1, moving in subarea (c) t = 2, moving in subarea (d) t = 3, crossing the boundary

Fig. 5. The Process of Grid Tracking

and SR_j are located respectively at two sides of a circle as it is shown in Fig. 2;

(4) Given this circle is the boundary of Anchor A and Anchor B, the sequence AB(BA) will become BA(AB) when entering(leaving). Thus, the sequence of A and B is still after crossing the circle(including entering and leaving) as it is shown in Fig. 2.

So it is possible that one signature owns more than one sub-region. ■

To eliminate the error rate and improve the accuracy, minimizing the vicious division is a considerable step in EFD's anchors placement scheme. N_v denotes the number of vicious division, and N_s is the total number of subareas, $S = \{S_1, S_2, ...S_{N_s}\}$. The optimal anchor placement scheme in EFD will satisfy: Maximize N_s, Subject to $N_s > 1$, and Minimize N_v. Note that, in practice, this problem can be solved by a bootstrapping technique [20].

D. Grid Tracking Strategy

As mentioned previously, one of challenges that the EFD system faces is the status quo issue. In this section, we will discuss another key technique in EFD, the grid tracking strategy [21], [22]. Denote $\vec{V}_t$ as the estimated velocity of the target at time t and $\vec{D}_t$ as the moving direction of the target. These two properties, describing the motion, can be estimated precisely by approaches such as the geomagnetic field analysis in the EFD location platform.

While the target is moving, fictitious edges for four two-dimensional directions, S, N, W, and E, are dynamically created to gauge the motion range of a target at each cycle t. By default, the edges matrix L are set to the boundary ($\mathbb{B}_n$) of the Subarea A_n in Equation 13

$$L(0) = \mathbb{B}_n = \begin{pmatrix} \min(x) & \max(x) \\ \min(y) & \max(y) \end{pmatrix}, (x, y) \in A_n \tag{13}$$

(x, y) is the coordinates of the subarea A_i that the target enters initially. Then, the L at time t is updated by Equation 14,

$$L(t) = L(t-1) + \bar{V} \cdot \vec{D} \tag{14}$$

If the edge L exceeds the boundary of subarea A_i, this L will be replaced with the boundary. The reciprocal process is demonstrated in Fig. 5. Note that the process continues until a detection of a signature change, which indicates that the target is crossing the boundary of the subarea. To move the L, we define a velocity matrix Lv as in Equation 15

$$Lv = \begin{bmatrix} \bar{V} \cdot \cos\theta & \bar{V} \cdot \cos\theta \\ \bar{V} \cdot \sin\theta & \bar{V} \cdot \sin\theta \end{bmatrix} \tag{15}$$

If a target moves within one subarea, $L(t) = L(t-1) + Lv$. However, once it crosses the boundary, the limit L will make a specific change.

E. Correction with Boundary Passing

When a target crosses a boundary separating two subareas S_i and S_j, based on theorem 1, the corresponding signature from EFD's mobile localization platform will change. This change actually offers a chance for EFD to calibrate the location estimation. Denote D_v as the direction indicator in Equation 16:

$$D_v = \begin{pmatrix} we & sn \end{pmatrix} \tag{16}$$

in which, we=$(\frac{1}{2}\pi < \theta < \frac{3}{2}\pi)$?1:2, sn=$(\pi < \theta < 2\pi)$?1:2, and $\theta = \angle\vec{D}$. Once the signature changes, the correction algorithm will be carried out immediately as described in Algorithm 1.

Algorithm 1: Correction at Boundary Crossing

Output: $L \rightarrow$the limit for estimated position
1 Input area sequence number n
2 Get $\mathbb{B}_n$ as defined in Equation 13
3 Get the estimated angle for current moving (θ) to calculate the Dir and Lv
4 $temp = L + Lv$
5 **for** $i = 1; i \leq 2$ **do**
6 **if** $temp_{i,j}$, $j = 3 - Dir_{1,i}$ *inside subarea* **then**
7 L_{ij}=$temp_{i,j}$
8 **else**
9 $UsedBorder \leftarrow \mathbb{B}_n(i, 3 - Dir_{1,i})$
10 $L_{i,j}$= $UsedBorder$
11 $L_{i,Dir_{1,i}}$=$L_{i,3-Dir_{1,i}}$+$2Lv_{i,Dir_{1,i}}$;
12 $estPos \leftarrow \frac{\sum(x_k, y_k)}{numberof(x_k, y_k)}$ where $(x_k, y_k) \in subarea(n)$&&$(x_k, y_k) \in Limit(t)$

VI. Lessons Learned

As discussed in Sections III, IV-B, V and, the EFD faces a practical problem–illegal signature. In our initial experiments, it is discovered that such an impasse scenario can destroy the robustness of EFD system. For example, in a practical scenario, we may receive a signature $s_m = (3, 4, 1, 2)$, but $s_m \notin \{s | s = \mathcal{F}(rss(i)), i = 1, 2, ..., N\}$. In an effort to ensure efficient use of the signature set S

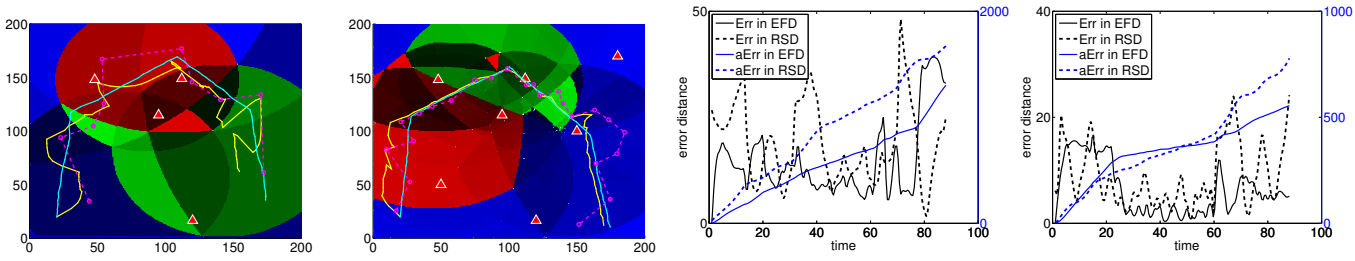

(a) N=4, v=4 (b) N=7, v=4 (c) N=4, v=4 (d) N=7, v=4

Fig. 6. The path and error distance when speed is four

by minimizing the impasse scenario, a utility function is introduced in Equation 17,

$$U(\hat{p}_i, \sigma^2_{\hat{p}_i}) = \hat{p}_i - \gamma\sigma^2_{\hat{p}_i} \tag{17}$$

where $\hat{p}$ is defined as the average of RSS from anchor i, $\sigma^2_{\hat{p}}$ is the standard deviation of $\hat{p}$, and γ defines a relative interference coefficient that describes the loss in signal strength due to environmental interference. The γ is higher in a signal unfriendly environment such as a concrete building than it will be in an outdoor environment with less interface. Therefore, to resolve impasse condition, signatures must be selected. Let's define the weight assigned to different anchors as $W = \{w_1, w_2, ..., w_n\}$ (w_i is the weight for $anchor_i$). As such, the optimization problem is to determine W so that the total utility is maximized, that is:

$$\begin{aligned} &\max_W \sum_i w_i U(\hat{\rho}_i, \sigma^2_{\hat{\rho}_i}) \\ &\text{s.t. } \sum w_i = 1 \text{(denotes as W'=1) and } w_i > 0 \end{aligned} \tag{18}$$

Under our definition, the total utility is written as:

$$\begin{aligned} \mu(W') &= \sum_{i=1}^{n} w_i U(\hat{\rho}_1, \sigma^2_{\hat{\rho}_i}) \\ &= \sum_{i=1}^{n} w_i\hat{\rho}_i - \gamma(\sum_{i=1}^{n} w_i^2\sigma^2_{\hat{\rho}_i} + 2\sum_{i=1}^{n}\sum_{j\neq i}^{n} w_i w_j Cov(\sigma_{\hat{\rho}_i}, \sigma_{\hat{\rho}_j})) \\ &= W'\rho - \gamma W'QW \end{aligned} \tag{19}$$

in which

$$Q = Cov(\sigma_{\hat{\rho}_i}, \sigma_{\hat{\rho}_j}) = \begin{bmatrix} \sigma^2_{\hat{\rho}_1} & \sigma_{\hat{\rho}_1,\hat{\rho}_2} & \cdots & \sigma_{\hat{\rho}_1,\hat{\rho}_n} \\ \sigma_{\hat{\rho}_2,\hat{\rho}_1} & \sigma^2_{\hat{\rho}_2} & \cdots & \sigma_{\hat{\rho}_1,\hat{\rho}_n} \\ \vdots & \vdots & \ddots & \vdots \\ \sigma_{\hat{\rho}_n,\hat{\rho}_1} & \sigma_{\hat{\rho}_n,\hat{\rho}_2} & \cdots & \sigma^2_{\hat{\rho}_n} \end{bmatrix} \tag{20}$$

$\sigma_{\hat{\rho}_i,\hat{\rho}_j}$ is the degradation correlation between anchors i and j, and n is the number of anchors. The numerical solution of W can be solved by Lagrangian derivation. Let's form Lagrangian function

$$L = W'\rho - \gamma W'QW - \lambda_1(W' - 1) \tag{21}$$

where λ_1 is a Lagrange multiplier. Then, taking derivatives of the Lagrangian with respect to vector W':

$$\frac{\partial L}{\partial W'} : \rho - \gamma QW - \lambda_1 = 0 \tag{22}$$

As a result, this proves Equation (23). The optimal $W = \{w_1, w_2..., w_n\}$ can then be applied to RSS to derive the optimal field signature.

Lemma 2. *The optimal solution of W will be:*

$$W = \frac{1}{\gamma}Q^{-1}(\rho - \lambda_1) \tag{23}$$

VII. System Evaluation by Comparisons

To illustrate the performance of the EFD system, we executed extensive computer simulations and conducted field tests based on our software-hardware EFD system platform. In this section, the simulation results are demonstrated, by comparing EFD with RSD and adjusting the estimated speed.

A. Evaluation Criterion

Before the simulation, we summarize the evaluation criterion for tracking. One is real-time error of localization, $Err(t)$ shown in Equation 24; another one is Accumulated Error, $aErr(t)$, which is defined in Equation 25.

$$Err(t) = \sqrt{(\hat{x} - X_g)^2 + (\hat{y} - y_g)^2} \tag{24}$$

$$aErr(t) = aErr(t-1) + Err(t) = \int_0^t Err(t); \tag{25}$$

in which $\hat{x}, \hat{y}$ are the estimated position coordinates and X_g, Y_g are the ground-truth position coordinates respectively; $t > 0$, and $aErr(0) = Err(0)$.

B. EFD VS. RSD with Multiple Anchors

In the first category of simulation, the velocity v is under controlled and the number of anchors N varies. As shown in Fig. 6, the green line represents the actual path of the target, the yellow line represents the calculated path by the EFD, and the pink line is the result from the RSD only. To get a numerical comparison between the RSD and the EFD, the error distance Err and the accumulative error distance $aErr$ are compared. Fig. 6 shows the performance metrics with $N = 4$. From the analysis of these figures, we can see clearly that the EFD outperforms the RSD in all scenarios. What's more, under poor anchors coverage, such as four anchors, the EFD can improve the accuracy of the system more dramatically. It is not surprised that when there are few anchors deployed, the subareas are larger on average, so the EFD, powered by grid tracking algorithm, can achieve higher localization resolution in almost every subarea.

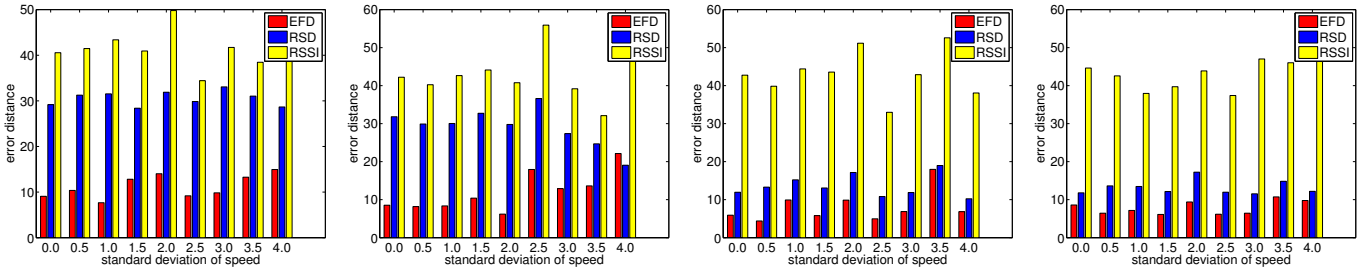

(a) N=4, v=4 (b) N=4, v=5 (c) N=7, v=4 (d) N=7, v=5

Fig. 7. Different Standard Deviation

C. Effects of Target Velocity

Considering that the estimated speed plays an important role in grid tracking, speed variation $v \sim N(\mu_v, \sigma_v^2)$ is another major factor that will affect the accuracy of the system. So we also show the results under different standard deviations(σ_v).(To eliminate the effect of estimated direction, our simulation set the real moving direction as the estimated one) Higher σ_v implies higher lability of the estimated volatility and hence can be used to evaluate real-time tracking system's performance. In this comparison, the σ_v varies from 0 to 4 speeding units, we then compare the results among the EFD, RSD and RSSI approaches and adjust the average speed and number of anchors. As shown in Fig. 7, the error distances caused by volatility, increase as σ_v increases. However, such error increase is alleviated if N increases and v decreases. In conclusion, the proposed EFD system still outperforms the RSD and RSSI in all of the speeding scenarios, rendering much lower localization errors than with other approaches.

VIII. Test-bed System Introduction

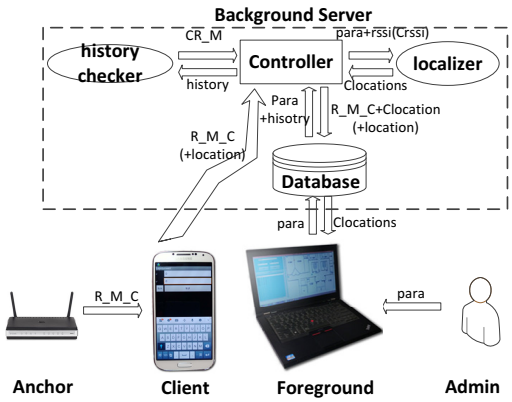

Fig. 8. The Relationship Between each Part of the experiment

In this section, we explain how modules in the EFD system work together. To cooperate with each of the other parts efficiently, there are three types of roles:

1) Administrator. It trains initial parameters of anchors and collecting in-situ information of scenarios.
2) Client (Receiver). It refers to the smart-phone receiving RSSs from anchors and collects magnetic information from sensors.
3) Anchor (Sender). It refers to s a low-cost signal emitter, like a wireless routers or a beacon.

The relationship between each part is shown in Fig. 8 (mainly for the measuring section) and the descriptions for messages are concluded in TABLE I. There are six

TABLE I. The Meaning of Message

R_M_C	RSS and Mac address from *Anchor*s with the ID of *Client*
CR_M_C	Adjusted RSS and Mac data using Weighted Map with the Client's ID
Clocation	Computed position of the *Client*
location	groud-truth position of the *Client*, an input from *Client* in training mode
para	Parameters of *Anchor*s and scenario, an input from *Admin*
history	history of R_M_C and Clocation

parts in the system, including two foregrounds in Android and PC and four kernel parts in Background Server.

1) Android-based smartphone:

- receive data from each anchor
- code the received data
- send the formatted R_M_C to the server

2) database(mysql): This part is used to store the data. During the localization period, it stores the Clocation and R_M_C(CR_M_C). During the training period, an additional value, the real position, denoted as *location*, is collected in this part. The *location* is an input from the Client (Trainer).

TABLE II. Database Design

target_x	computed position of the target x
anchor_tb	information of the anchor: mac and coordinate
site_para	scenario: length and width
log_target_x	log and data for target x

3) foreground display: Foreground display is a user-friendly part to display the tracking and help non-professional users.

4) The controller: this part is the kernel of the system, controlling the main flows and handling them in the Algorithm 2.

Algorithm 2: Controller works in measuring mode

Output: *Clocation,history*
Input: *R_M_C,para*
if *log_time==0* **then**
  read *para* from Tables anchor_tb and site_para in *Database*;
while *Receive R_M_C from* Client **do**
  if *log_time%LOG_NUM==0 and log_time!=0* **then**
    read *history* from *Database*;
    CR_M_C= History Checker(history);
    Clocation=Localize(CR_M_C,para);
    clear log_target_C;
    if *isValide(Clocation)* **then**
      write *Clocation* to Table target_C;
  else
    Clocation=Localize(R_M_C,para); write the *R_M_C, Clocation* to Table log_target_C;
  log_time++;

5) localizer: It is used to compute sequence and initialize the segmentation map after entering the *para* from the *Administrator*, it then gets the subarea of the *Client* using the RSS from *Anchors*, computes the estimated direction from magnetic data from *Client*'s sensor. Finally it returns the estimated coordinate of *Client* as Algorithm 1 shows.

6) history checker: It is used to checkout and fit the more appropriate RSS of anchors according to the previous records, and return the Checked RSSI. This is the implementation of optimal RSS utility.

IX. Localization System Platform Evaluation

To quantify the performance of the proposed EFD algorithm, we carried out extensive field tests by using our EFD localization system as shown in Fig. 8. An android-based Samsung I9500 smart-phone, is used as a mobile platform. Tenda w3200 Wi-Fi routers and self-designed wireless hotspots are used as the wireless anchors in following experiments. Our experiments are categorized into three sets in different environments with increasing complexity.

A. Planted in wide open area

In the first set, anchors were deployed in a wide open area, measuring 30 meters in length and 40 meters in width, as shown in Fig. 10. Target client moved randomly at a normal velocity of a pedestrian, and measured the localization errors at different spots. Under such specification, accumulated error distances of the RSD and the EFD are shown in Fig. 9(a). The results show that the EFD outperforms the RSD with almost 50 percent higher localization accuracy.

B. Experiments in a building

Secondly, we conducted an experiment in a complex environment, that included trees, stairs, pillars, and an aisle. Anchors were placed in the hallway of the parterres, as shown in Fig. 11. Tracking results are depicted

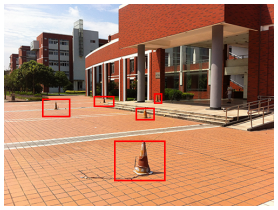

(a) Experiment Scenario 1

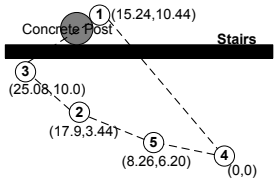

(b) Abstract Deployment 1

Fig. 10. Experiment in a wide open area

Fig. 11. Experiment in a More Complex Area

in Fig. 9(b), which indicates that the EFD achieved an average error 33.3 percent less than the RSD.

C. Experiments in a classroom

Fig. 12. Experiment in a Rather Complex Area

Third, we carried out experiments in classrooms where RF signals shading can be serious, because of the walls and numerous desks and chairs, as seen in Fig. 12. The tracking result, as shown in Fig. 9(c), also illustrates that the EFD outperforms the RSD with 15 percent lower error.

Thus, these experiments in Sections IX-A, IX-B, IX-C demonstrate EFD's relatively high interference-free capacity.

D. Comparison Evaluation

TABLE III. Comparison among four algorithms

Name	Accuracy	Weakness
EZ	2-7m	GPS Lock
Unloc	4-10m	intensive prior study
DV-hop	5-10m	considerable error distance
EFD	1-4m	low with large scale of anchors

Based on the overall results, we quantitatively compare the EFD with other algorithms, such as EZ [9], Unloc [10] and DV-hop [23]. Average error results are shown in TABLE III. Limited in equipment, We use only 802.11 whose stability is not high enough compared with GSM [24] in our experiments. As such, it is concluded that the EFD can achieve a better performance with less complexity and higher robustness for on-demand deployment, if using GSM.

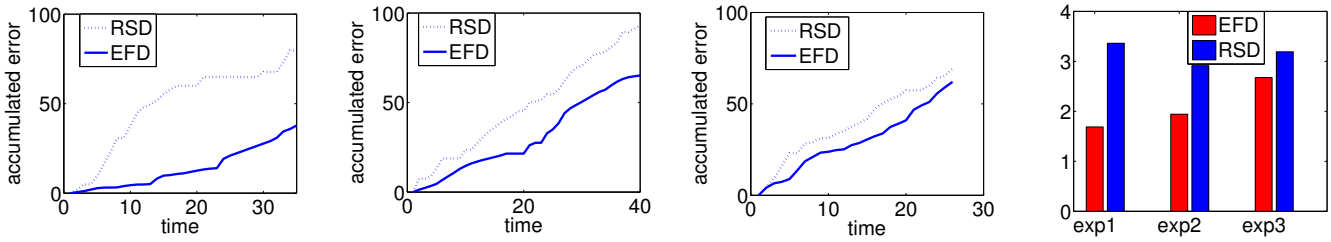

(a) Outdoor (b) Hallway (c) Classroom (d) Comparison

Fig. 9. The Results of Three Experiments (unit of error distance is meter)

X. Conclusion

This paper introduces a new mechanism of localization called Enhanced Field Division (EFD), which increases the accuracy and stability of the system within terrains with high interference. Based on the division signatures, which can track the target's position within the possible subarea using estimated direction and walking speed, is proposed as a complement for signature-only EFD. This is an important attempt in which both sender and receiver play roles in localization. In addition, three strategies are also introduced to minimize illegal signatures, vicious field division and Status Quo Effects.

To verify the EFD, we conduct a series of simulations, and build a real-environmental localization system. The results prove that the EFD is more accurate and reliable than other approaches, like the RSD, DV-Hop and unLoc. Besides, there is great potential to spread the EFD algorithm using popular transmitters like iBeacons.

XI. Acknowledgements

This work is supported in part by NSFC(61431008, 61300217, 61271220, 61170164), NSF CNS(1503590), Natural Science Foundation of Shanghai(15ZR1423600), 973 program(2013CB329603), State Engineering Laboratory for Information Content Analysis Technology(GT036001), and Hunan University Junior Scholar Development Fund.

References

[1] R. Stoleru, T. He, and J. A. Stankovic, "Range-free localization," in *Secure Localization and Time Synchronization for Wireless Sensor and Ad Hoc Networks*. Springer, 2007, pp. 3–31.

[2] T. He, C. Huang, B. M. Blum, J. A. Stankovic, and T. Abdelzaher, "Range-free localization schemes for large scale sensor networks," in *Proceedings of the 9th annual international conference on Mobile computing and networking*. ACM, 2003, pp. 81–95.

[3] J. Pan, L. Cai, Y. T. Hou, Y. Shi, and S. X. Shen, "Optimal base-station locations in two-tiered wireless sensor networks," *Mobile Computing, IEEE Transactions on*, vol. 4, no. 5, pp. 458–473, 2005.

[4] L. Ding, X. Gao, W. Wu, W. Lee, X. Zhu, and D.-Z. Du, "Distributed construction of connected dominating sets with minimum routing cost in wireless networks," in *Distributed Computing Systems (ICDCS)*. IEEE, 2010, pp. 448–457.

[5] C. Wang, J. Chen, Y. Sun, and X. Shen, "Wireless sensor networks localization with isomap," in *ICC*. IEEE, 2009, pp. 1–5.

[6] H. Ammari, J. Garnier, and K. Sølna, "A statistical approach to target detection and localization in the presence of noise," *Waves in Random and Complex Media*, vol. 22, no. 1, pp. 40–65, 2012.

[7] Z. Zhong and T. He, "Achieving range-free localization beyond connectivity," in *Proceedings of the 7th ACM Conference on Embedded Networked Sensor Systems*. ACM, 2009, pp. 281–294.

[8] P. Chen, Z. Zhong, and T. He, "Bubble trace: Mobile target tracking under insufficient anchor coverage," in *Distributed Computing Systems (ICDCS)*. IEEE, 2011, pp. 770–779.

[9] K. Chintalapudi, A. Padmanabha Iyer, and V. N. Padmanabhan, "Indoor localization without the pain," in *Proceedings of the sixteenth annual international conference on Mobile computing and networking*. ACM, 2010, pp. 173–184.

[10] H. Wang, S. Sen, A. Elgohary, M. Farid, M. Youssef, and R. R. Choudhury, "Unsupervised indoor localization," *Duke University*, 2012.

[11] M. T. Isik and O. B. Akan, "A three dimensional localization algorithm for underwater acoustic sensor networks," *Wireless Communications, IEEE Transactions on*, vol. 8, no. 9, pp. 4457–4463, 2009.

[12] K. Yedavalli and B. Krishnamachari, "Sequence-based localization in wireless sensor networks," *Mobile Computing, IEEE Transactions on*, vol. 7, no. 1, pp. 81–94, 2008.

[13] S. Basagni, M. Nati, and C. Petrioli, "Localization error-resilient geographic routing for wireless sensor networks," in *Global Telecommunications Conference, 2008. IEEE GLOBECOM 2008. IEEE*. IEEE, 2008, pp. 1–6.

[14] G. Wu, S. Wang, B. Wang, Y. Dong, and S. Yan, "A novel range-free localization based on regulated neighborhood distance for wireless ad hoc and sensor networks," *Computer Networks*, 2012.

[15] P. Yi, M. Yu, Z. Zhou, W. Xu, Q. Zhang, and T. Zhu, "A three-dimensional wireless indoor localization system," *Journal of Electrical and Computer Engineering*, p. 13, 2014.

[16] A. Malekpour, T. Ling, and W. Lim, "Location determination using radio frequency rssi and deterministic algorithm," in *Communication Networks and Services Research Conference, 2008. CNSR 2008. 6th Annual*. IEEE, 2008, pp. 488–495.

[17] C. Papamanthou, F. P. Preparata, and R. Tamassia, "Algorithms for location estimation based on rssi sampling," in *Algorithmic Aspects of Wireless Sensor Networks*. Springer, 2008, pp. 72–86.

[18] C. V. Durell, *Modern geometry: the straight line and circle*. Macmillan and Company, 1920.

[19] Q. Zhang, G. Sobelman, and T. He, "Gradient-driven target acquisition in mobile wireless sensor networks," in *Mobile Ad-hoc and Sensor Networks*. Springer, 2006, pp. 365–376.

[20] L. P. Clare, G. J. Pottie, and J. R. Agre, "Self-organizing distributed sensor networks," in *AeroSense'99*. International Society for Optics and Photonics, 1999, pp. 229–237.

[21] M. S. Cohen and S. Y. Bookheimer, "Localization of brain function using magnetic resonance imaging," *Trends in Neurosciences*, vol. 17, no. 7, pp. 268 – 277, 1994.

[22] Q. Zhang, L. Fu, T. Zhu, Y. Gu, P. Yi, and J. Chen, "Mobile anchor assisted error bounded sensing in sensor networks: An implementation perspective," in *Mobile Ad-Hoc and Sensor Systems (MASS), 2013 IEEE 10th International Conference on*. IEEE, 2013, pp. 592–596.

[23] D. Niculescu and B. Nath, "Dv based positioning in ad hoc networks," *Telecommunication Systems*, vol. 22, no. 1-4, pp. 267–280, 2003.

[24] A. Varshavsky, E. de Lara, J. Hightower, A. LaMarca, and V. Otsason, "Gsm indoor localization," *Pervasive and Mobile Computing*, vol. 3, no. 6, pp. 698–720, 2007.